

Orbital periods of twenty two subdwarf B stars

L. Morales-Rueda¹, P. F. L. Maxted^{2,1}, T. R. Marsh¹, R. C. North^{1,3}, U. Heber⁴

¹*Department of Physics and Astronomy, University of Southampton, UK (lmr@astro.soton.ac.uk, trm@astro.soton.ac.uk)*

²*School of Chemistry and Physics, Keele University, UK (pflm@astro.keele.ac.uk)*

³*Meteorological Office, London Road, Bracknell, Berkshire, RG12 2SZ, UK*

⁴*Dr Remeis-Sternwarte, Astronomisches Institut der Universität Erlangen-Nürnberg, Sternwarstrasse 7, 96049 Bamberg, Germany*

Accepted 0000 000 00; Received 0000 000 00; in original form 0000 000 00

ABSTRACT

Subdwarf B (sdB) stars are thought to be core helium burning stars with low mass hydrogen envelopes. In recent years it has become clear that many sdB stars lose their hydrogen through interaction with a binary companion and continue to reside in binary systems today. In this paper we present the results of a programme to measure orbital parameters of binary sdB stars. We determine the orbits of 22 binary sdB stars from 424 radial velocity measurements, raising the sample of sdBs with known orbital parameters to 38. We calculate lower limits for the masses of the companions of the sdB stars which, when combined with the orbital periods of the systems, allow us to discuss approximate evolutionary constraints. We find that a formation path for sdB stars consisting of mass transfer at the tip of the red giant branch followed by a common envelope phase explains most, but not all of the observed systems. It is particularly difficult to explain both long period systems and short period, massive systems. We present new measurements of the effective temperature, surface density and surface helium abundance for some of the sdB stars by fitting their blue spectra. We find that two of them (PG0839+399 and KPD1946+4340) do not lie in the Extreme Horizontal Branch (EHB) band indicating that they are post-EHB stars.

Key words:

binaries: close – binaries: spectroscopic – subdwarfs

1 INTRODUCTION

Subdwarf B (sdB) stars can be identified with models for Extreme Horizontal Branch (EHB) stars. The surface gravities and temperatures of sdB stars suggest that they have helium cores of mass $\sim 0.5 M_{\odot}$ and thin hydrogen envelopes of mass $\leq 0.02 M_{\odot}$ (Heber et al. 1984; Saffer et al. 1994). A recent asteroseismological study of an sdB star results in a value for its mass of $0.49 \pm 0.02 M_{\odot}$ (Brassard et al. 2001). Several evolutionary scenarios have been proposed to explain the formation of sdB stars, in particular the loss of the hydrogen envelope. Evolution within a binary star is an effective method for envelope removal, and yet it is hard to see why this should have happened to a horizontal branch star since it would have been much larger during its preceding red giant stage. A solution to this problem was presented by D’Cruz et al. (1996) who found that if a red giant star with a degenerate helium core loses its hydrogen envelope when it is within ~ 0.4 magnitudes of the tip of the red giant branch, the core can go on to ignite helium, despite the dramatic mass loss, and may then appear as an sdB star. The advantage of this model is that it very nicely explains the

masses of sdB stars as a consequence of the core mass at the helium flash. D’Cruz et al. (1996) supposed that mass loss occurred because of an enhancement of the stellar wind, but it could as well have been driven by binary interaction.

If sdB stars do form within binary systems and if they still have their companions, then the companions must be low-mass main-sequence stars or compact stellar remnants to avoid outshining the sdB star. If so, it is probable that in many cases the companions were unable to cope with the mass transferred from the sdB progenitor and a single “common” envelope formed around the two stars. Driving off such envelopes drains energy and angular momentum from the binary orbit, which as a result becomes much smaller than it was at the start of mass transfer (Webbink 1984). It is therefore possible that many sdB stars are now members of close binary systems. Maxted et al. (2001) found exactly this, discovering 21 binary sdB stars in a sample of 36, suggesting, after allowance for detection efficiency, that some two-thirds of all sdB stars are in short period binary systems ($P \lesssim 10$ d). The other third seems to be made up a combination of long period binary stars that avoided a

common envelope phase (Green, Liebert & Saffer 2000) and apparently single sdB stars.

If D’Cruz et al.’s (1996) model of the formation of sdB stars is correct, then the stage immediately prior to mass transfer in binary sdBs is well defined. This, together with the fact that the binary does not have enough time to change its orbital period significantly following its emergence from the common envelope, makes the sdB stars a superb population for testing models of the common envelope phase. Moreover, the detection of sdB binary stars is not compromised by the strong and poorly understood selection effects that plague other populations of close binary stars, such as the cataclysmic variable stars. The properties of sdB binaries (e.g. their orbital period distribution) can be compared fairly directly with the results of binary population synthesis codes and are therefore a strong test of population synthesis models for binary stars.

Following on from the detection of many binary stars by Maxted et al. (2001), we started a project to measure their orbits. The orbit of one of the new binary stars has been presented in Maxted et al. (2002a). In this paper we present the orbits of a further 22 systems. We then consider the implications of the known sdB binary stars for their evolution. It should be noted that our sample is biased against sdB stars with G/K-type companions as the majority of our stars were selected from the PG survey which excludes most stars that show a CaII H-line.

2 OBSERVATIONS AND REDUCTION

The data used in this study were taken with the Intermediate Dispersion Spectrograph (IDS) at the 2.5m Isaac Newton Telescope (INT) on the island of La Palma. Two different configurations of the IDS were used for the observations. The first setup consisted of the 500 mm camera with the R1200R grating centred in H α and the TEK (1kx1k) Charge couple device (CCD) giving a dispersion of 0.37 Å/pix and a resolution of 0.9 Å. The second setup used the 235 mm camera with the R1200B grating centred at 4350Å and the thinned EEV10 (2kx4k) CCD covering the Balmer lines from H β to H ϵ , giving a dispersion of 0.48 Å/pix and a resolution of 1.4 Å. We carried out the observations during six different runs. The dates when the observations were taken and the setup used during each campaign are given in Table 1. We took two consecutive observations of each object and bracketed them with CuAr plus CuNe frames to calibrate the spectra in wavelength. We subtracted from each image a constant bias level determined from the mean value in its over-scan region. Tungsten flatfield frames were obtained each night to correct for the pixel to pixel response variations of the chip. Sky flatfields were also obtained to correct for the pixel to pixel variations of the chip along the slit. After debiasing and flatfielding the frames, spectral extraction proceeded according to the optimal algorithm of Marsh (1989). The arcs were extracted using the profile associated with their corresponding target to avoid systematic errors caused by the spectra being tilted. Uncertainties on every point were propagated through every stage of the data reduction.

Table 1. Journal of observations. Setup 1 is: INT + IDS + 500 mm + R1200R + λ_c =H α . Setup 2 is: INT + IDS + 235 mm + R1200B + λ_c =4350Å.

Dates	Setup	# of RV observations
10 – 21 Apr 2000	1	85
5 – 6 Feb 2001	1	28
8 – 13 Mar 2001	1	130
1 – 8 May 2001	1	99
6 – 11 Aug 2001	2	56
27 Sep – 6 Oct 2001	2	26

3 RESULTS

3.1 Radial velocity measurements

To measure the radial velocities we used least squares fitting of a model line profile. The model line profile is the summation of three Gaussian profiles with different widths and depths. For any given star, the widths and depths of the Gaussians are optimised and then held fixed while their velocity offsets from the rest wavelengths of the lines in question are fitted separately for each spectrum; see Maxted, Marsh & Moran (2000c) for further details of this procedure. For the data taken on the April 2000, the February, March, and May 2001 observing runs, the fitting was performed to the H α line whereas for the August and September 2001 observing campaigns, the fitting was carried out simultaneously to all the Balmer lines present in the spectra. Table 6 gives a list of the radial velocity measurements for the 22 objects presented in this paper.

Using the measured radial velocities of the lines, we determined the orbital periods of our targets. The description of the orbital period determination is given in Section 3.2. The results of folding the radial velocities of each object on its orbital period are plotted in Fig. 1. The error bars on the radial velocity points are, in most cases, smaller than the size of the symbol used to display them. For that reason we also display the residuals of the fit on a scale 10 times larger than the scale of the radial velocity curves. We find that there is no sign of ellipticity in any of the radial velocity curves, not even at long periods where departures from circular orbits might be expected. This is good evidence for the action of the common envelope. The values of the orbital periods, systemic velocities and radial velocity semi-amplitudes for each system are given in Table 2.

3.2 Determination of orbital periods

We use a “floating mean” periodogram to determine the periods of our targets (e.g. Cumming, Marcy & Butler 1999). The method consists in fitting the data with a model composed of a sinusoid plus a constant of the form:

$$\gamma + K \sin(2\pi f(t - t_0)),$$

where f is the frequency and t is the observation time. The key point is that the systemic velocity is fitted at the same time as K and t_0 . This corrects a failing of the well-known Lomb-Scargle (Lomb 1976; Scargle 1982) periodogram which starts by subtracting the mean of the data and then fits a plain sinusoid; this is incorrect for small numbers of points.

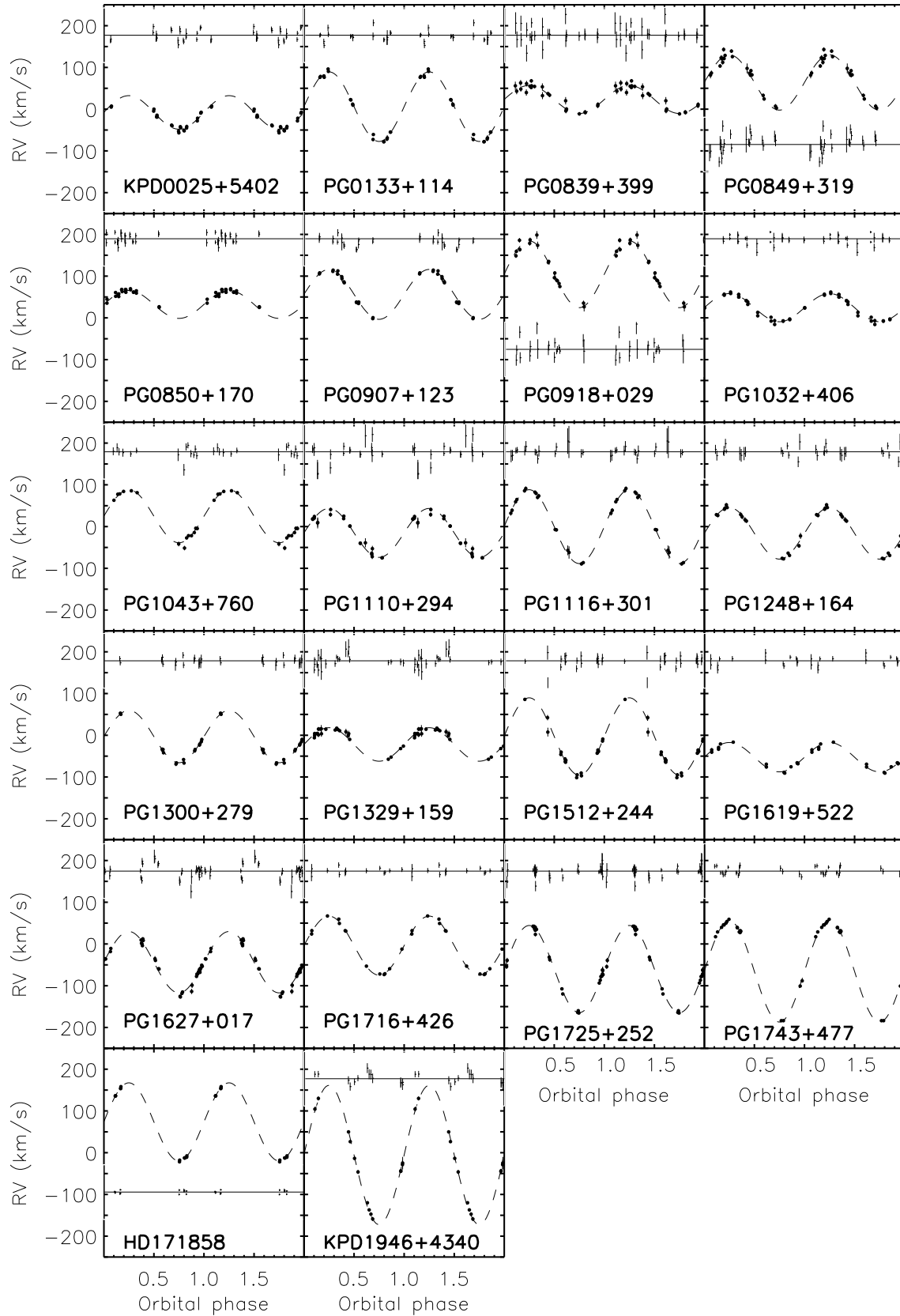


Figure 1. Each panel presents the radial velocity curve measured for each object. The data have been folded on the orbital period in each case. See table 2 for the list of periods, radial velocity semiamplitudes and systemic velocities. Included in each panel is a plot of the residuals to the fit. The vertical scale on which the residuals have been plotted is 10 times larger than the scale on which the radial velocities are plotted.

Table 2. List of the orbital periods measured for the 22 sdBs studied. T_0 , the systemic velocity, γ , the radial velocity semi-amplitude, K , the reduced χ^2 achieved for the best alias, the 2nd best alias and the χ^2 difference between the 1st and 2nd aliases are also presented. The number of data points used to calculate the orbital period is given in the final column under n . See text for a comment on the orbital period of PG1043+760.

Object	HJD (T_0) –2450000	Period (d)	γ (km/s)	K (km/s)	$\chi^2_{reduced}$	2nd best alias (d)	$\Delta\chi^2$	n
KPD0025+5402	2159.386(9)	3.571(1)	-7.8 ± 0.7	40.2 ± 1.1	2.82	3.832(2)	21	22
PG0133+114	2158.682(2)	1.2382(2)	6.0 ± 1.0	83.2 ± 0.8	2.13	4.277(1)	129	18
PG0839+399	1914.06(6)	5.622(2)	23.2 ± 1.1	33.6 ± 1.5	1.22	4.720(1)	16	24
PG0849+319	1841.992(3)	0.74507(1)	64.0 ± 1.5	66.3 ± 2.1	1.94	0.426983(6)	22	20
PG0850+170	1834.3(2)	27.81(5)	32.2 ± 2.8	33.5 ± 3.1	1.44	13.86(2)	13	23
PG0907+123	1840.62(3)	6.1163(6)	56.3 ± 1.1	59.8 ± 0.9	1.13	5.0619(5)	30	16
PG0918+029	1842.310(4)	0.87679(2)	104.4 ± 1.7	80.0 ± 2.6	1.87	0.82644(3)	53	18
PG1032+406	1888.66(2)	6.779(1)	24.5 ± 0.5	33.7 ± 0.5	1.63	6.034(1)	16	24
PG1043+760	1842.4877(7)	0.1201506(3)	24.8 ± 1.4	63.6 ± 1.4	1.62	0.572097(5)	40	14
PG1110+294	1840.49(3)	9.415(2)	-15.2 ± 0.9	58.7 ± 1.2	1.50	1.16397(3)	32	21
PG1116+301	1920.834(2)	0.85621(3)	-0.2 ± 1.1	88.5 ± 2.1	0.52	4.5237(8)	26	16
PG1248+164	1959.853(4)	0.73232(2)	-16.2 ± 1.3	61.8 ± 1.1	0.93	0.688431(7)	21	16
PG1300+279	1908.310(7)	2.2593(1)	-3.1 ± 0.9	62.8 ± 1.6	0.65	1.50254(4)	26	16
PG1329+159	1840.579(1)	0.249699(2)	-22.0 ± 1.2	40.2 ± 1.1	0.92	0.199694(2)	17	23
PG1512+244	1868.521(2)	1.26978(2)	-2.9 ± 1.0	92.7 ± 1.5	0.81	0.363261(1)	37	20
PG1619+522	1837.0(1)	15.357(8)	-52.5 ± 1.1	35.2 ± 1.1	1.38	0.1153123(3)	23	14
PG1627+017	2001.267(1)	0.829226(8)	-43.7 ± 0.5	73.6 ± 0.9	2.63	0.836541(8)	413	32
PG1716+426	1915.806(5)	1.77732(5)	-3.9 ± 0.8	70.8 ± 1.0	0.78	2.62356(6)	75	13
PG1725+252	1901.3977(8)	0.601507(3)	-60.0 ± 0.6	104.5 ± 0.7	1.08	0.594906(3)	512	30
PG1743+477	1921.1183(7)	0.515561(2)	-65.8 ± 0.8	121.4 ± 1.0	1.44	1.024201(6)	58	18
HD171858	2132.241(6)	1.529(8)	73.8 ± 0.8	93.6 ± 0.7	0.65	0.6352(8)	28	12
KPD1946+4340	2159.0675(5)	0.403739(8)	-5.5 ± 1.0	167.0 ± 2.4	1.49	0.400780(8)	78	14

We obtain the χ^2 of the fit as a function of f and then identify minima in this function. Section 3.3 gives a detailed explanation on the probability of the periods obtained being incorrect.

Table 2 gives a list of the orbital parameters derived for each sdB binary star. The orbital period of the second best period is also given, along with the difference in χ^2 between the two best periods found. The resulting periodograms (χ^2 versus orbital frequency) are given in Figs. 2 and 3. Each panel includes an blow up of the region in frequency where the minimum χ^2 is found. It is clear from the figures that in all cases, apart from PG1043+760, the difference in χ^2 between the best and the second alias is at least 10. We have made an exception for PG1043+760, because in this case the competing aliases are so close (owing to 1 cycle/year aliasing) that it makes more sense to consider the nearest competing group of aliases.

3.3 The probability that our periods are incorrect

A sometimes frustrating characteristic of radial velocity work is that while one can very soon know for sure that a star is binary – perhaps after just two measurements – it can take much longer to pin down the orbital period. One somehow has to know when the orbital period is “correct”. To compound this problem, another feature of radial velocity orbits is that if one picks an incorrect alias, the period can be *completely* wrong, even when the quoted uncertainty on the best-fit period is tiny. This is simply because the statistics are not Gaussian so that an error of 100 or even 1000 times quoted uncertainty can happen. Perhaps the most common way around this issue is the “method of overkill” where one

takes so much data as to put the issue beyond any doubt, but this is necessarily inefficient. This is a particular problem with the sdB stars where there is no shortage of potential targets, but always a shortage of telescope time in which to observe them. Our approach whilst observing was to use the rule-of-thumb that an orbit was determined once the best-fit orbit improved upon the next-best by at least 10 in χ^2 . The basis for this is that the probability of a period in the Bayesian sense is dominated by the term $\exp -\chi^2/2$ (see the appendix), and so a difference of more than 10 shows that the second-best alias is at least $\exp 5 \approx 150$ times less probable than the best. This rule-of-thumb was propagated into the submitted version of the paper, but the referee made two cogent criticisms of this approach. First, while the peak of the second alias may be > 150 times less probable than the peak of the best alias, there is no guarantee that the total probability of *any* other period was as low. Second, some of our χ^2 values were larger than expected given the number of data points, suggesting some extra source of uncertainty that if included would reduce one’s faith in the best alias.

Both of these criticisms were justified, and the first in particular prompted us to develop a more rigorous approach which we describe below. To address the second point we have computed the level of systematic uncertainty that when added in quadrature to our raw error estimates gives a reduced $\chi^2 = 1$. The reasoning behind this is that there may be an un-accounted source of error such as true variability of the star or slit-filling errors causing the poor fits of a few stars. It seems unlikely that such errors will be either correlated with the orbit or with the statistical errors we estimate, and therefore we add a fixed quantity in quadrature with our statistical errors as opposed to applying a simple

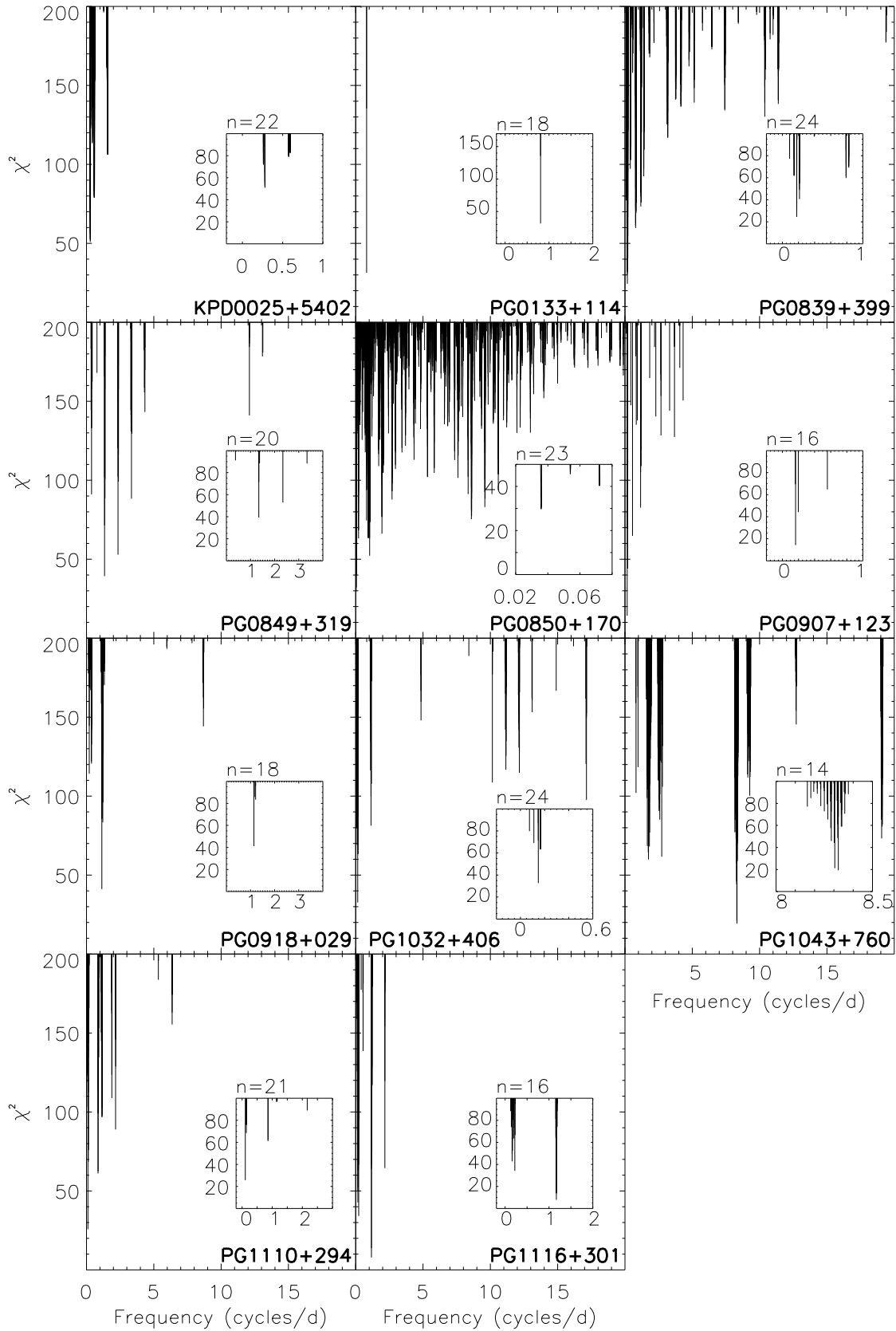


Figure 2. Each panel presents χ^2 versus cycles/day obtained after the period search was carried out. The frequency with the smallest χ^2 corresponds to the orbital frequency of the system. For clarity we have also included an inset showing a blow up of the region where the best period is. The number of radial velocity measurements used for the period search calculations, n , is shown in each panel.

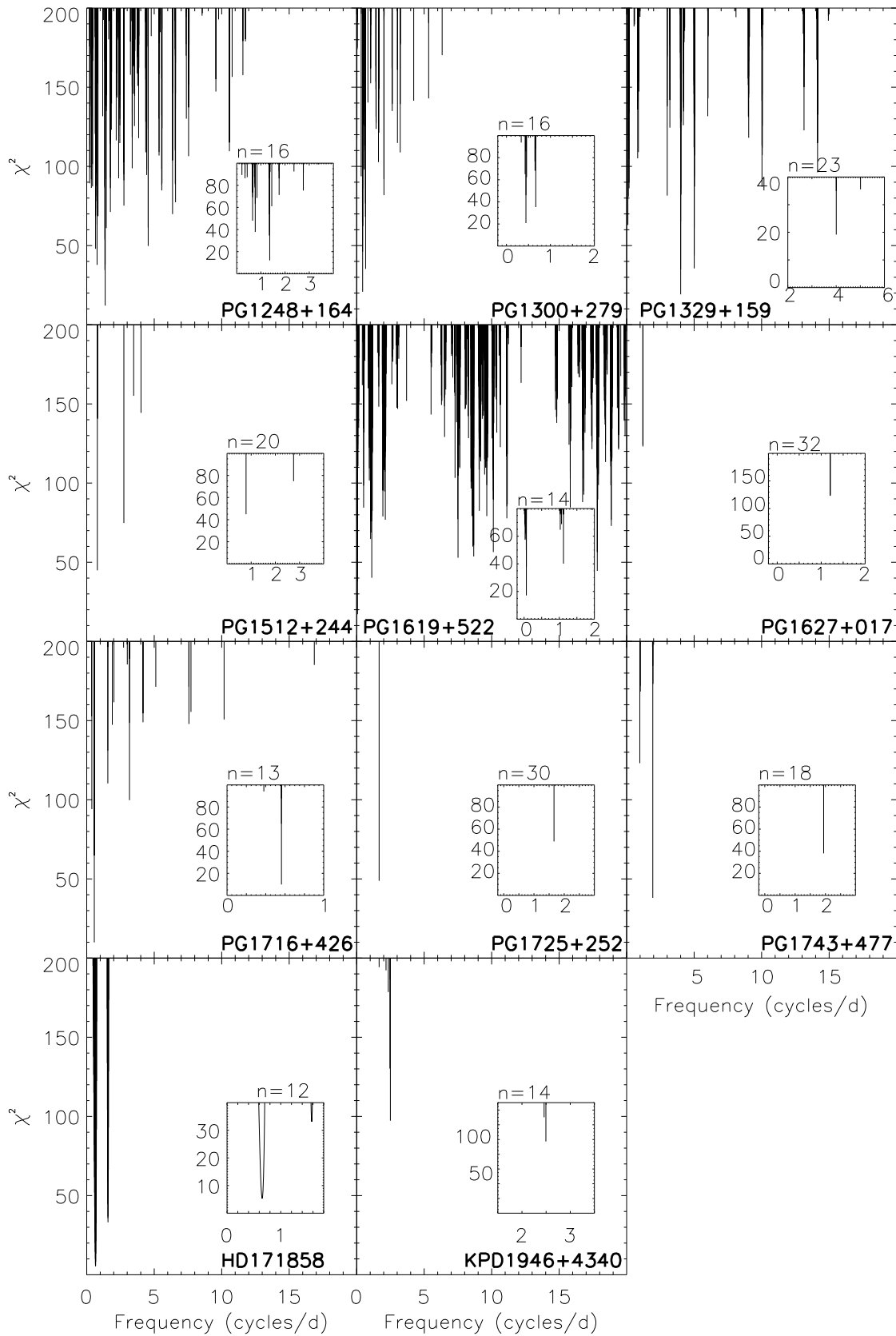


Figure 3. Same as in Fig. 2 for the remaining 11 systems.

multiplicative scaling to them. In all cases we use a minimum value of 2 km s^{-1} corresponding to $1/10^{\text{th}}$ of a pixel which we believe to be a fair estimate of the true limits of our data.

The end result is that in two cases there is indeed a relatively large probability that our periods are in error (KPD0025+5402; PG1032+406), nevertheless we continue to list them in this paper on the bases that (a) the best periods remain strongly favoured in all cases and therefore are probably correct and (b) the IDS spectrograph is being withdrawn from service and it is not clear when we will get the opportunity to gather more data. These systems (KPD0025+5402, PG1032+406) therefore come with a health warning: there is a larger than desirable probability that we may not have picked the best alias for them.

In most cases the probability of the orbital period being further than 1 and 10 per cent from our favoured value is the same. This is because all the significant probability lies within a very small range around the best period, with all the significant competition (i.e. next best alias) placed outside the 10 per cent region around the best alias. In the case of HD171858, the probability of the true orbital period being further than 1 per cent from the one given in this paper is very high. This is due to the short baseline of our observations (1 day) which means that the period is not determined anything like as well as the others and in particular is not confined to within 1 per cent of the best fit. For the purpose of comparing observations to evolutionary models there is no need for better than 10 per cent measurements and we are quite certain that the period is correct within those limits. The probabilities for all systems are listed in Table 3 where we give the logarithm (base 10) of the chance that the true period lies further than 1 and 10 per cent of our favoured value.

To calculate these probabilities, we integrated equation A4 from the appendix of Marsh, Dhillon & Duck (1995). Full details of our method are given in the appendix to this paper. The calculation is Bayesian, and therefore involves prior probabilities over all parameters, i.e. the systemic velocity, semi-amplitude, phase and period. These ‘‘priors’’ are uncertain and therefore the final probabilities listed in Table 3 are similarly uncertain. This we believe is the main reason why one would like the probability of being incorrect to be *very* small, so as to overcome any plausible uncertainty in the prior probabilities; this is one justification for the method of overkill. For most of our sample, this is in fact the case, but we feel that the uncertainties are large enough to leave a grain of doubt when the probability listed in Table 3 rises above 0.1%, or -3 in the log, as it does for the two stars discussed.

4 DISCUSSION

4.1 Effective temperature, surface gravity and helium abundance

For those sdBs that we observed in the blue, we measured the effective temperature, T_{eff} , the surface gravity, $\log g$, and the helium abundance, $\log(\text{He}/\text{H})$. We used Saffer et al.’s (1994) procedure to fit the profiles of the Balmer, the He I and the He II lines present in the spectra by a grid of

Table 3. List of probabilities that the true orbital period of a system lies further than 1 and 10 per cent from our favoured value given in Table 1. Numbers quoted are the logs in base 10 of the probabilities. Column number 4 gives the value of the systematic uncertainty that has been added in quadrature to the raw error to give a χ^2 that lies above the 2.5 per cent probability in the χ^2 distribution.

Object	1%	10%	systematic error (km s^{-1})
KPD0025+5402	-1.32	-2.29	5
PG0133+114	-15.80	-15.80	3
PG0839+399	-3.73	-3.73	2
PG0849+319	-4.19	-4.19	3
PG0850+170	-3.05	-3.39	2
PG0907+123	-5.04	-5.04	2
PG0918+029	-4.66	-9.16	3
PG1032+406	-2.03	-2.03	3
PG1043+760	-4.74	-4.74	2
PG1110+294	-6.66	-6.66	2
PG1116+301	-4.75	-4.75	2
PG1248+164	-4.60	-4.92	2
PG1300+279	-5.70	-5.70	2
PG1329+159	-3.57	-3.57	2
PG1512+244	-7.26	-7.26	2
PG1619+522	-5.24	-5.24	2
PG1627+017	-55.94	-68.89	4
PG1716+426	-5.17	-5.17	2
PG1725+252	-104.88	-124.42	2
PG1743+477	-26.45	-26.45	2
HD171858	-0.28	-6.88	2
KPD1946+4340	-12.96	-15.32	2

synthetic spectra. The synthetic spectra obtained from hydrogen and helium line blanketed NLTE atmospheres (Napiwoztki 1997) were matched to the data simultaneously. For stars cooler than 27 000 K we used the metal line-blanketed LTE model atmospheres of Heber, Reid, & Werner (2000). Before the fitting was carried out, we convolved the synthetic spectra with a Gaussian function to account for the instrumental profile. See Heber et al. (2000) for details of the models. The values of T_{eff} , $\log g$, and $\log(\text{He}/\text{H})$ for some of the objects are the same as those presented by Maxted et al. (2001). Those that are different from the ones obtained by Maxted et al. (2001) and those for which T_{eff} and $\log g$ have not been calculated previously (KPD0025+5402 and KPD1946+4340) are given in Table 4.

All the objects from Table 4 apart from two lie in or near the band defined by the zero-age extreme horizontal branch (ZAEHB), the terminal-age extreme horizontal branch (TAEHB) and the He main sequence (HeMS) and are therefore extreme horizontal branch stars (EHB). (See Fig. 2 of Maxted et al. (2001) for a $\log g$ versus T_{eff} plot for the objects not included in Table 4.) The two objects that lie outside the EHB band are post-EHB stars. PG0839+399 appears in Saffer et al. (1994) as an EHB star, and KPD1946+4340 is a new post-EHB star.

4.2 Orbital parameters known up to now

Table 5 gives a list of all of the orbital parameters of sdB binary stars known to date. In each case we require that both the orbital period and the radial velocity semi-amplitude are

Table 4. T_{eff} , $\log g$ and $\log(\text{He}/\text{H})$ calculated for newly discovered sdB binaries (KPD0025+5402 and KPD1946+4340). We also present these values for other systems when they do not coincide with previously published measurements (Maxted et al. 2001).

Name	T_{eff} (K)	$\log g$	$\log(\text{He}/\text{H})$	Model
KPD0025+5402	28200	5.37	-2.9	NLTE
PG0101+039	27300	5.50	-2.7	NLTE
PG0133+114	29600	5.66	-2.3	NLTE
PG0839+399	37800	5.53	-3.7	NLTE
PG1627+017	21600	5.12	-2.9	LTE
PG1716+426	26100	5.33	-2.9	LTE
PG1743+477	27600	5.58	-1.8	NLTE
HD171858	27700	5.25	-2.9	NLTE
KPD1946+4340	34500	5.37	-1.35	NLTE

measured. We combine the orbital periods and the radial velocity semi-amplitudes to calculate the mass function, f_m , of the system according to the well-known relation:

$$f_m = \frac{M_2^3 \sin^3 i}{(M_1 + M_2)^2} = \frac{PK_1^3}{2\pi G},$$

where the subscript “1” refers to the sdB star and “2” to its companion.

If we take a canonical mass of $0.5 M_\odot$ for the sdB star, we can also calculate the minimum mass of its companion, $M_{2\text{min}}$. The values for f_m and $M_{2\text{min}}$ obtained in each case are given in Table 5. We have also added in the table a column indicating the nature of the companion, where known, i.e. whether it is a compact object (most likely a white dwarf, indicated by “WD”) or a non-degenerate object (a main sequence star or a brown dwarf, indicated by “MS”). The evolution of each type is fundamentally different since in the first case the system must go through at least two mass transfer episodes whereas in the second case the system suffers only one mass transfer episode. It is notable that all the sdB stars with “MS” companions have very short orbital periods.

In Fig. 4 we present a histogram of all the known orbital periods of sdBs. The dashed line shows the systems with previously published periods and the solid line shows the combination of the previously published periods and the ones measured in this work. There is no sign of any fine structure such as the well-known “period gap” of the cataclysmic variable stars. The main points to take from this plot are the large dynamic range and that our survey has substantially increased the numbers of long period systems ($P > \text{a few days}$). This is probably a consequence of the large time base of our data.

Fig. 5 shows $M_{2\text{min}}$ versus orbital period, assuming $M_1 = 0.5 M_\odot$. All the systems given in Table 5 are included in the plot. The systems whose periods are measured in this paper are plotted as asterisks whereas sdB binaries with previously published orbital periods are plotted as plus signs. In addition, to test the idea of mass loss followed by a common envelope shortly before the helium flash, we present limits based upon a common envelope phase initiated when the progenitor of the sdB star was at the tip of the red giant branch. We calculate the effect of the common envelope in the standard fashion (Webbink 1984) with a fraction α_{CE} of the loss of orbital energy set equal to the binding energy

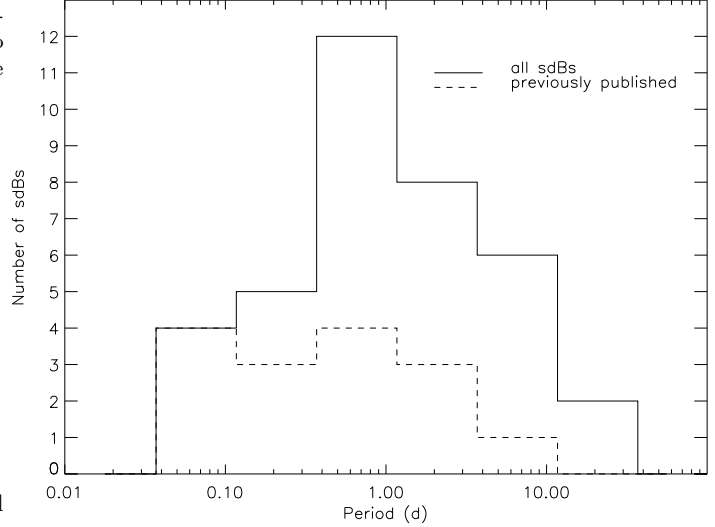


Figure 4. Histogram of orbital periods for all the sdB binaries known up to now.

of the envelope. We apply the standard mass transfer equations instead of those calculated by Nelemans et al. (2001) because in most cases we are treating the second phase of mass transfer instead of the first phase. The change in orbital energy is

$$\Delta E_{\text{orb}} = \frac{GM_1 M_2}{2a_i} - \frac{GM_{\text{sdB}} M_2}{2a_f},$$

where M_1 is the mass of the sdB star’s progenitor and a_i and a_f are the initial and final orbital separations. Parameterising the envelope binding energy as

$$E_{\text{env}} = -\frac{GM_1(M_1 - M_{\text{sdB}})}{\lambda R_1},$$

where λ depends upon the structure of the envelope and the contribution of internal as well as gravitational energy (Dewi & Tauris 2000). We then have

$$\alpha_{\text{CE}} \lambda \left(\frac{GM_{\text{sdB}} M_2}{2a_f} - \frac{GM_1 M_2}{2a_i} \right) = \frac{GM_1(M_1 - M_{\text{sdB}})}{R_1}.$$

Thus given M_1 , M_2 , M_{sdB} , R_1 and the combination $\alpha_{\text{CE}} \lambda$, the final separation can be computed for any given initial separation.

Following this formalism, the different lines in the plots represent the following constraints:

(i) the leftmost curve represents the limit imposed by the lack of mass transfer in these binaries. The limit has been calculated assuming that the companion is a main sequence star and therefore does not apply for white dwarf companions. We have used Eggleton’s (1983) formula for the Roche lobe radius to obtain this limit.

(ii) the curve marked with $M_1 > 1.9 M_\odot$ marks the limit beyond which there would be no helium flash. We have employed Hurley et al.’s (2000) analytic formulae to calculate how large the progenitor of the sdB was, assuming that mass transfer occurred near the tip of the RGB. For a given initial mass, metallicity and common envelope efficiency one can then predict the current period as a function of M_2 , assuming that the sdB star has a mass of $0.5 M_\odot$ at the end.

Table 5. List of all the sdBs with known orbital periods. The radial velocity semi-amplitude K , the minimum mass of the donor star $M_{2\min}$, the mass function f_m , and the companion type, either main sequence “MS” or white dwarf “WD”, when known, are also given. A “WD” companion could actually be a white dwarf, a neutron star or another compact object. ¹ indicates recent measurements looking for reflection effects in the lightcurves by Maxted et al. (2002b). 22 out of the 38 periods are measured in this paper. References for the other orbital periods given are (a) Moran et al. 1999, (b) Maxted et al. 2000a, (c) Dreschel et al. 2001, (d) Orosz & Wade 1999, (e) Maxted et al. 2000b, (f) Wood & Saffer 1999, (g) Napiwotzki et al. 2001, (h) Saffer, Livio & Yungelson 1998, (i) Kilkeny et al. 1998, (j) Edelman, Heber & Napiwotzki (2001), (k) Maxted et al. 2002a, (l) Foss, Wade & Green 1991. * Edelman, Heber & Napiwotzki (2001) measure values for this system consistent with the values presented in this paper.

Object	P_{orb} (d)	K (km s ⁻¹)	$M_{2\min}$ (M_{\odot})	f_m (M_{\odot})	WD/MS	Ref.
PG0001+275	0.528	90.0	0.293	0.040		j
KPD0025+5402	3.571	40.2	0.235	0.024		
PG101+039	0.569908	104.3	0.370	0.067	WD	a
PG0133+114	1.2382	83.2	0.388	0.074		*
KPD0422+5421	0.09017945	237.0	0.499	0.124	WD	d
HS0705+6700	0.095646643	85.8	0.136	0.006	MS	c
PG0839+399	5.622	33.5	0.226	0.022		
PG0849+319	0.7451	66.2	0.228	0.022	WD ¹	
PG0850+170	27.81	33.5	0.466	0.108		
PG0907+123	6.1163	59.8	0.521	0.136		
PG0918+029	0.87679	79.9	0.313	0.046	WD ¹	
PG0940+068	8.330	61.2	0.634	0.198		b
PG1017-086	0.0729939	49.3	0.066	0.001	MS	k
PG1032+406	6.779	33.7	0.247	0.027		
PG1043+760	0.1201506	63.6	0.106	0.003	WD ¹	
HE1047-0436	1.213253	94.0	0.458	0.104	WD	g
PG1101+249	0.35386	134.6	0.424	0.089	WD	h
PG1110+294	9.415	58.7	0.633	0.197		
PG1116+301	0.85621	88.5	0.356	0.062	WD ¹	
HW Vir	0.116720	82.3	0.140	0.007	MS	f
PG1247+554	0.602740	32.2	0.090	0.002		b
PG1248+164	0.73232	61.7	0.207	0.018	WD ¹	
PG1300+279	2.2593	62.7	0.346	0.058		
PG1329+159	0.249699	40.2	0.083	0.002	MS ¹	
PG1336-018	0.1010174	78.0	0.125	0.005	MS	i
PG1432+159	0.22489	120.0	0.294	0.040	WD	a
PG1512+244	1.26978	92.7	0.458	0.105		
PG1538+269	2.501	88.3	0.600	0.179	WD	h, l
PG1619+522	15.357	35.2	0.376	0.069		
PG1627+017	0.829226	73.5	0.273	0.034		
PG1716+426	1.77732	70.8	0.366	0.065		
PG1725+252	0.601507	104.5	0.381	0.071		
UVO1735+22	1.278	103.0	0.539	0.145		j
PG1743+477	0.515561	121.3	0.438	0.095		
HD171858	1.529	93.6	0.510	0.130		
KPD1930+2752	0.095111	349.3	0.967	0.420	WD	e
KPD1946+4340	0.403739	166.9	0.628	0.195		
PG2345+318	0.2409458	141.2	0.379	0.070	WD	a

Massive companions get rid of the envelope easily and therefore end up at long periods. To get short periods and high companion masses one needs some combination of inefficient envelope ejection, a small red giant and a massive envelope. The latter two conditions occur for large mass progenitors since the radius at the tip of the giant branch decreases with mass for low mass stars. This sets a lower limit on the progenitor mass; $M_1 = 1.9 M_{\odot}$ is taken as the maximum since above this the core is not degenerate and there is then no natural explanation for the $\log g/T_{\text{eff}}$ distribution of sdB stars.

(iii) the vertical line on the right hand side is the upper limit on the final period given that the sdB progenitor mass had to be $\gtrsim 1 M_{\odot}$ for it to have evolved to this stage within the lifetime of the Galaxy.

(iv) the maximum value for M_2 has been chosen to be $1.4 M_{\odot}$, corresponding to the Chandrasekhar stellar limit. Any main sequence star this massive would be easily visible.

(v) the dashed line that appears at the bottom of the figures indicates the minimum M_2 required to get the smallest amplitude that we can detect ($\sim 10 \text{ km s}^{-1}$). This crudely shows that selection effects are likely to be weak in our data.

In addition to show the sensitivity to variations of these limits, we show the case for $M_1 < 1.75 M_{\odot}$ and $M_2 < 0.65 M_{\odot}$. Most of the data are contained within these more restrictive limits. It should be remembered when looking at these plots that the companion masses are lower limits owing to the unknown orbital inclinations of most targets.

Three panels are shown to show the effect of varying either the metallicity [Fe/H] (which affects the radius of the

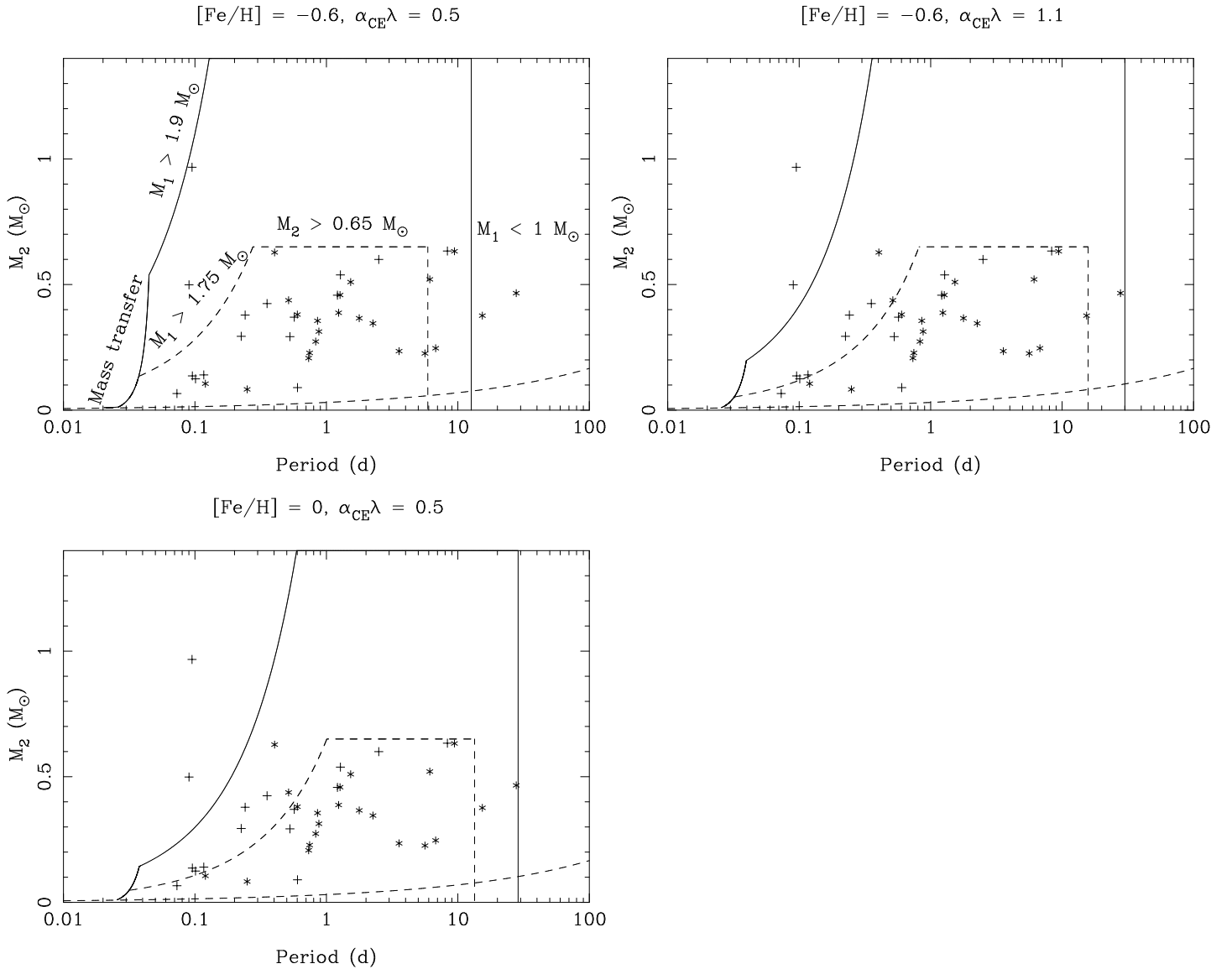


Figure 5. Mass of the companion star versus orbital period. The sdB binaries whose periods are measured in this paper are represented by a * symbol whereas systems with previously published periods are represented by a +. We have also included in the plot different constraints. These are explained in detail in the text. The three panels present 3 different combinations of two parameters, the metallicity, $[\text{Fe}/\text{H}]$, and the common envelope efficiency, $\alpha_{\text{CE}}\lambda$.

star) or the common envelope efficiency/envelope structure parameter, $\alpha_{\text{CE}}\lambda$. Increasing the metallicity increases the radius at mass transfer and results in longer period systems being formed. This is also the result if the efficiency with which orbital energy is used to expel the common envelope increases. The largest value of $\alpha_{\text{CE}}\lambda$ used in our calculations is 1.1. If the value of $\alpha_{\text{CE}}\lambda = 2$, favoured by Nelemans et al. (2001), is considered, this results in even longer period systems being formed.

The conclusion to be drawn from all this is that although a common envelope phase as a result of mass loss immediately prior to the helium flash covers the range of parameters of most systems, it does not explain simultaneously systems of long orbital period and systems of short orbital period with massive companions. The two systems KPD1930+2752 ($P = 0.0951$ d, $M_2 > 0.97 M_{\odot}$) and KPD0422+5421 ($P = 0.0902$ d, $M_2 > 0.50 M_{\odot}$) look partic-

ularly discrepant and may require an alternative formation path, such as a descent from progenitors with $M_1 > 2 M_{\odot}$.

4.3 sdB stars with main-sequence companions

Five of the short period sdB binary stars are known to have main-sequence or brown dwarf companions. All of them have very short periods indeed, with PG1329+159 having the longest period at 4.0 hr. This fits with the low masses of their companions, $\sim 0.1 M_{\odot}$ compared to $\sim 0.5 M_{\odot}$ for a typical white dwarf. It also suggests an interesting possibility for the 10 – 20 percent of sdB stars that are apparently single (Maxted et al. 2001; Green et al. 2000): perhaps these stars could be the result of merging of even lower mass companions, unable to survive the common envelope phase. This would at least avoid the need to have a single star route for sdB formation to supplement the binary star route which

already seem to account for 80 to 90 percent of these stars. The long period sdB/main-sequence binaries identified by Green et al. (2000) must have avoided a common envelope. Perhaps they could do so because their relatively high mass main-sequence components were able to accrete at a high enough rate to avoid the common envelope. It would be of great interest to measure element abundances in the main-sequence components of these stars, e.g. abundance ratios of $^{12}\text{C}/^{13}\text{C}$ (Sarna et al. 1995).

5 CONCLUSIONS

We have confirmed the binary nature of 22 subdwarf B stars and have measured their orbital parameters. This work increases the sample of sdB binaries with known orbital parameters to 38. The observations extend over several months allowing us to detect orbital periods of the order of tens of days, longer than any previously measured.

We have measured T_{eff} , $\log g$, $\log(\text{He}/\text{H})$ for the sdBs where previous measurements of these quantities did not exist. When we place the results in the $T_{\text{eff}}\text{-}\log g$ plot we find that two out of the 22 sdBs are post-EHB stars.

The large range of orbital periods and companion masses is a challenge to simple theories for the formation of sdB stars. Although binary-induced mass-loss at the tip of the red giant branch is able to explain most systems, it appears unlikely to be the only formation route. Full population synthesis will be needed to establish the viability of alternative paths.

Amongst sdB stars with known orbits, those with low-mass main-sequence or brown dwarf companions have particularly short periods. It seems likely that a fraction of such systems, particularly those of very low companion mass, may not have survived the common envelope phase. We suggest that these could now be the single sdB stars.

ACKNOWLEDGEMENTS

LMR was supported by a PPARC post-doctoral grant. The reduction and analysis of the data were carried out on the Southampton node of the STARLINK network. The Isaac Newton Telescope is operated on the island of La Palma by the Isaac Newton Group in the Spanish Observatorio del Roque de los Muchachos of the Instituto de Astrofísica de Canarias. We thank PATT for their support of this program.

REFERENCES

- Brassard P., Fontaine G., Billeres M., Charpinet S., Liebert J., Saffer R. A., 2001, *ApJ*, 563, 1013
 Cumming A., Marcy G. W., Butler R. P., 1999, *ApJ*, 526, 890
 D’Cruz N. L., Dorman B., Rood R. T., O’Connell R. W., 1996, *ApJ*, 466, 359
 Drechsel H., Heber U., Napiwotzki R., Ostensen R., Solheim J-E., Johannessen F., Schuh S. L., Deetjen J., Zola S., 2001, *A&A*, 379, 893
 Dewi J. D. M., Tauris T. M., 2000, *A&A*, 360, 1043
 Edelmann H., Heber U., Napiwotzki R., 2001, *AN*, 322, 401
 Eggleton P. P., 1983, *ApJ*, 268, 368
 Foss D., Wade R. A., Green R. F., 1991, *ApJ*, 374, 281

- Green E. M., Liebert J., Saffer R. A., 2000, Proceedings of the Twelfth European Workshop on White Dwarfs. ASP Conference Series, in press (astro-ph/0012246)
 Heber U., Hunger K., Jonas G., Kudritzki R. P., 1984, *A&A*, 130, 119
 Heber U., Reid I. N., Werner K., 2000, *A&A*, 363, 198
 Hurley J. R., Pols O. R., Tout C. A., 2000, *MNRAS*, 315, 543
 Kilkenny D., O’Donoghue D., Koen C., Lynas-Gray A. E., van Wyk F., 1998, *MNRAS*, 296, 329
 Lomb N. R., 1976, *Ap&SS*, 39, 447
 Marsh T. R., 1989, *PASP*, 101, 1032
 Marsh T. R., Dhillon V. S., Duck S. R., 1995, *MNRAS*, 275, 828
 Maxted P. F. L., Heber U., Marsh T. R., North R. C., 2001, *MNRAS*, 326, 139
 Maxted P. F. L., Marsh T. R., Morales-Rueda L., *MNRAS*, 2002b, in preparation
 Maxted P. F. L., Marsh T. R., Heber U., Morales-Rueda L., North R. C., Lawson W. A., 2002a, *MNRAS*, 333, 231
 Maxted P. F. L., Marsh T. R., Moran C. K. J., 2000c, *MNRAS*, 319, 305
 Maxted P. F. L., Marsh T. R., North R. C., 2000b, *MNRAS*, 317, 41
 Maxted P. F. L., Moran C. K. J., Marsh T. R., Gatti A. A., 2000a, *MNRAS*, 311, 877
 Moran C., Maxted P., Marsh T. R., Saffer R. A., Livio M., 1999, *MNRAS*, 304, 535
 Napiwotzki R., 1997, *A&A*, 322, 256
 Napiwotzki R., Edelmann H., Heber U., Karl C., Drechsel H., Pauli E-M., Christlieb N., 2001, *A&A*, 378, 17
 Nelemans G., Yungelson L. R., Portegies Zwart S. P., Verbunt F., 2001, *A&A*, 365, 491
 Orosz J. A., Wade R. A., 1999, *MNRAS*, 310, 773
 Saffer R. A., Bergeron P., Koester D., Liebert J., 1994, *ApJ*, 432, 351
 Saffer R. A., Livio M., Yungelson L. R., 1998, *ApJ*, 502, 394
 Sarna M. J., Dhillon V. S., Marsh T. R., Marks P. B., 1995, *MNRAS*, L41
 Scargle J. D., 1982, *ApJ*, 263, 835
 Wood J. H., Saffer R., 1999, *MNRAS*, 305, 820
 Webbink R. F., 1984, *ApJ*, 277, 355

APPENDIX A: THE PROBABILITY OF BEING WRONG

Marsh, Dhillon & Duck (1995) derived the following equation (their A4) for the probability of a binary star of orbital frequency f versus a single star given a set of radial velocity data, D

$$\frac{P(B, f|D)}{P(S|D)} = \frac{P(B, f)}{P(S)} \frac{4(2\pi)^{3/2}}{R_K^2 R_\gamma (\det \mathbf{A})^{1/2}} \frac{R_\gamma (\sum_i w_i)^{1/2}}{(2\pi)^{1/2}} \times \exp \frac{1}{2} \left(\mathbf{b}^t \mathbf{A}^{-1} \mathbf{b} - \frac{(\sum_i w_i \mathbf{V}_i)^2}{\sum_i w_i} \right),$$

where the vector \mathbf{b} is given by

$$\mathbf{b} = \begin{pmatrix} \sum_i w_i \\ \sum_i w_i c_i \\ \sum_i w_i s_i \end{pmatrix}, \quad (\text{A1})$$

and the matrix \mathbf{A} is

$$\mathbf{A} = \begin{pmatrix} \sum_i w_i & \sum_i w_i c_i & \sum_i w_i s_i \\ \sum_i w_i c_i & \sum_i w_i c_i^2 & \sum_i w_i c_i s_i \\ \sum_i w_i s_i & \sum_i w_i s_i c_i & \sum_i w_i s_i^2 \end{pmatrix}, \quad (\text{A2})$$

Table 6. Radial velocities measured for the 22 sdBs.

HJD -2450000	RV (km s ⁻¹)	HJD -2450000	RV (km s ⁻¹)	HJD -2450000	RV (km s ⁻¹)	HJD -2450000	RV (km s ⁻¹)
PG0133+114		PG0849+319		PG1032+406		PG1116+301	
2128.5749	-72.7±3.5	2037.4053	125.8±4.1	1649.3760	-6.8±4.5	1653.5014	-89.4±3.9
2128.5785	-60.7±3.1	PG0850+170		1649.3776	-15.8±3.6	1653.5164	-86.4±2.8
2131.6335	76.2±1.8	1646.4208	69.8±2.0	1651.4124	24.5±2.5	1656.5285	82.5±3.0
2131.6406	78.4±1.9	1646.4333	67.3±2.2	1651.4141	23.4±2.5	1656.5386	79.3±2.8
2131.6824	79.6±2.5	1654.3966	26.6±2.4	1946.5069	13.0±4.5	1946.5774	32.0±5.7
2131.6861	76.4±2.5	1654.4067	25.1±2.3	1946.5088	5.0±3.4	1946.5884	39.0±4.9
2131.7340	96.2±2.9	1946.4409	35.3±3.4	1978.5666	61.9±1.5	1977.5184	85.8±4.5
2131.7376	90.5±2.7	1946.4518	44.6±3.0	1978.5701	58.4±1.5	1977.5288	91.2±4.9
2133.6602	-78.3±2.0	1977.3953	54.7±2.3	1979.6294	41.4±1.3	1977.6297	69.9±4.4
2133.6638	-77.6±2.0	1977.4057	56.0±2.3	1979.6329	40.8±1.3	1977.6401	73.5±5.0
2133.7420	-55.0±2.1	1977.5829	51.1±3.7	1979.7281	38.2±2.4	1978.6363	-7.2±3.1
2133.7456	-54.8±2.1	1977.5933	57.5±3.4	1979.7305	32.2±2.6	1978.6468	-7.9±3.9
2180.7593	-71.7±4.6	1978.3974	67.3±3.5	1982.5671	-2.7±2.0	1978.7442	-56.9±11.7
2180.7629	-68.8±6.7	1978.4078	68.1±2.9	1982.5695	-4.4±1.9	1978.7547	-62.1±14.7
2181.5733	12.0±2.3	1978.5355	62.9±3.1	2032.3651	56.7±2.2	1982.5794	59.4±2.7
2181.5769	9.6±3.3	1979.4663	68.1±2.2	2032.3698	54.3±2.4	1982.5898	64.8±2.8
2187.7392	22.9±1.9	1979.4767	62.9±2.3	2033.3479	56.2±3.2	PG1248+164	
2187.7428	22.1±1.9	1979.5629	67.5±3.2	2033.3503	55.5±2.5	1646.5672	41.5±2.0
PG0839+399		1979.5681	61.2±3.5	2033.3536	50.1±2.4	1646.5875	45.5±1.9
1646.3498	53.5±8.3	1982.4753	64.8±2.6	2033.3560	49.7±2.3	1656.5529	-63.6±3.2
1646.3562	32.4±8.4	1982.4857	59.2±2.4	2035.5349	1.5±1.1	1656.5632	-69.2±3.2
1651.3528	67.9±4.5	2032.4352	60.7±2.1	2035.5419	-7.8±1.1	1946.6313	-46.2±4.9
1651.3677	55.9±4.2	2032.4560	51.7±1.8	2036.3546	-7.8±4.3	1946.6422	-22.4±7.5
1654.3695	-7.0±4.9	2037.4162	62.0±2.2	2036.3570	-7.8±3.7	1977.6948	28.9±6.3
1654.3820	-8.2±4.6	2037.4266	61.2±2.1	PG1043+760		1977.7052	23.5±5.9
1946.3902	-11.3±4.2	PG0907+123		1649.3849	-27.1±3.3	1982.7060	44.0±4.6
1977.3520	55.1±3.6	1647.4116	86.4±2.9	1649.3959	-4.0±3.4	1982.7164	52.0±4.4
1977.4229	52.0±3.5	1647.4323	84.1±2.5	1651.4332	-21.9±3.3	2036.5834	-76.1±3.2
1977.6104	54.4±4.4	1653.3980	98.6±4.3	1651.4402	-4.8±3.2	2036.5939	-77.3±3.2
1978.3634	37.1±4.7	1653.4084	94.1±7.2	1978.5149	77.4±4.2	2037.5674	28.5±4.2
1978.4527	33.7±5.0	1654.4213	34.4±3.7	1978.5219	84.2±3.7	2037.5779	26.7±4.5
1979.3939	-1.2±4.6	1654.4351	37.9±2.1	1979.4291	-41.6±5.7	2038.5088	16.4±6.1
1979.4044	0.3±4.6	1946.4705	111.4±2.3	1979.4360	-51.5±5.3	2038.5193	13.3±4.6
1982.4504	62.9±7.1	1946.4849	114.4±2.7	1979.6126	85.7±2.6	PG1300+279	
1982.4608	48.1±6.4	1978.4914	37.9±2.6	1979.6195	81.2±2.6	1646.6051	53.0±2.4
2033.3690	39.8±7.6	1978.5053	36.6±2.5	1979.7118	63.0±3.6	1646.6166	50.2±2.3
2033.3795	61.1±6.8	1979.4910	-1.8±1.8	1979.7188	78.3±3.3	1656.6042	-33.9±2.6
2037.3763	7.9±5.3	1979.5049	0.5±1.8	2035.5512	-21.8±2.8	1656.6156	-41.9±2.5
2037.3868	11.4±5.2	1982.3503	105.4±3.5	2035.5581	-14.4±2.6	1946.6580	-15.3±5.0
2038.3738	56.0±10.0	1982.3642	107.8±3.7	PG1110+294		1946.6690	-10.1±4.0
2038.4482	43.1±7.4	2032.3927	104.7±2.2	1653.4747	8.7±13.1	1977.7172	-69.0±4.9
2181.7460	20.2±8.8	2032.4136	112.6±3.3	1653.4845	9.6±10.3	1977.7276	-66.2±3.7
2181.7602	-4.2±5.7	PG0918+029		1656.5069	1.2±2.9	1979.6646	-33.3±2.6
PG0849+319		1647.4808	35.3±5.9	1656.5167	1.3±2.9	1979.6750	-36.0±2.8
1646.3657	92.2±4.3	1647.4861	26.4±11.1	1657.4808	-39.8±3.1	1982.6567	-37.4±3.1
1646.3733	82.2±4.2	1653.3633	96.2±5.0	1657.4906	-40.1±3.1	1982.6672	-33.9±3.3
1651.3816	121.2 ±4.1	1653.3669	107.5±4.5	1946.5472	28.6±5.5	1982.7663	-23.4±4.4
1651.3891	128.7±4.1	1977.4392	148.6±5.1	1946.5633	40.8±4.6	1982.7732	-20.8±4.5
1946.4116	103.4±4.6	1977.4428	159.4±4.5	1978.6659	-64.0±4.5	2036.6295	-58.2±2.9
1946.4191	122.8±6.5	1978.3468	185.9±5.5	1978.6764	-66.6±4.3	2036.6405	-66.6±2.8
1946.4268	121.5±6.8	1978.3503	163.6±5.0	1978.7165	-72.0±5.9	PG1329+159	
1977.3726	7.0±5.3	1978.4363	178.6±5.4	1978.7304	-52.9±6.8	1646.6683	-1.2±3.1
1977.3798	2.7±5.4	1978.4398	186.9±5.4	1979.6421	-74.8±2.7	1646.6720	-9.9±3.0
1978.3795	81.5±7.7	1978.5994	132.8±4.8	1979.6526	-74.9±2.8	1656.6277	17.0±2.2
1978.3865	86.6±6.1	1978.6029	135.1±4.0	1982.5328	18.6±2.7	1656.6351	10.9±2.2
1978.4704	112.1±5.5	1979.5487	90.5±2.5	1982.5433	17.4±2.8	1947.7337	1.2±5.6
1978.4774	142.9±5.2	1979.5556	88.7±2.7	1982.6798	20.1±3.8	1947.7411	3.7±7.4
1979.4152	85.8±3.3	2036.3670	198.5±9.2	1982.6903	24.1±4.4	1977.6529	-31.8±3.1
1979.4221	81.4±3.8	2036.3740	173.7±8.9	2032.5190	19.0±2.4	1977.6599	-25.9±3.2
1982.3773	97.7±11.8	2037.4384	82.2±2.4	2032.5346	25.0±3.4	1978.6865	-6.0±2.9
1982.4969	33.0±4.3	2037.4453	75.1±2.6	2034.5643	-38.9±10.8	1978.6934	4.2±3.2
1982.5039	24.6±4.4					1978.7651	8.3±7.2
2037.3983	139.1±4.4					1978.7721	3.9±7.1

Table 6. continued.

HJD -2450000	RV (km s ⁻¹)	HJD -2450000	RV (km s ⁻¹)	HJD -2450000	RV (km s ⁻¹)	HJD -2450000	RV (km s ⁻¹)
PG1329+159		PG1627+017		PG1725+252		HD171858	
1979.6859	-0.3±2.6	1653.6236	-125.4±3.6	1651.7613	-62.2±6.7	2132.4162	135.8±0.8
1979.6929	4.3±2.2	1653.6261	-126.9±3.5	1651.7629	-63.7±9.5	2132.4186	136.5±0.8
1982.6163	-57.4±2.4	1654.6144	-66.6±2.7	1653.7578	40.1±3.7	2132.4211	136.1±0.8
1982.6233	-52.3±2.3	1654.6169	-68.0±2.8	1653.7610	39.7±4.7	2132.4974	153.5±0.9
2033.4229	12.6±2.9	1978.7757	-113.8±6.2	1654.7494	-93.5±1.8	2132.4998	154.8±0.8
2033.4298	13.6±2.7	1978.7792	-98.9±6.8	1654.7554	-86.7±2.0	2132.5023	158.2±0.8
2033.6309	14.9±5.1	2032.7251	-71.9±1.7	1977.7686	-78.2±3.3	2133.3961	-21.9±0.9
2033.6379	15.5±8.9	2032.7321	-66.7±1.7	1977.7721	-77.3±3.2	2133.3985	-17.8±0.9
2033.6493	14.6±4.2	2032.7397	-61.4±1.7	1979.7769	36.7±2.2	2133.4728	-12.3±1.3
2034.6203	4.3±2.0	2032.7464	-59.1±2.3	1979.7804	32.8±2.3	2133.4752	-13.0±1.3
2034.6342	14.8±1.7	2033.5451	-77.7±2.2	1979.7839	34.2±2.4	2133.5059	-10.9±0.8
	PG1512+244	2033.5486	-72.2±2.4	1979.7880	34.9±2.9	2133.5083	-7.6±0.8
1653.5782	-101.6±3.2	2033.6187	-35.5±2.2	1982.7842	36.8±3.5	KPD0025+5402	
1653.5837	-94.7±3.0	2033.6222	-36.1±2.2	1982.7865	39.9±3.6	2129.6652	-38.2±2.2
1657.6469	-42.9±2.8	2033.6614	-18.3±3.5	1982.7888	22.9±4.7	2129.6792	-40.0±2.6
1657.6525	-41.0±2.8	2033.6650	-10.7±3.3	2032.6991	42.5±1.8	2130.7039	-9.4±2.2
1946.6963	-46.0±3.2	2035.5739	9.5±2.1	2032.7061	42.4±1.7	2130.7180	-7.5±2.2
1946.7003	-40.3±3.2	2035.5774	2.0±2.1	2032.7130	39.9±1.7	2132.5951	-4.7±2.5
1978.6991	-90.4±4.1	2035.5814	0.0±2.2	2033.5694	-164.0±2.4	2132.6057	0.0±2.5
1978.7026	-97.0±4.0	2035.5849	-4.0±2.6	2033.5729	-159.9±2.5	2132.7141	-14.5±3.1
1979.7629	-56.4±2.9	2036.7411	-118.5±1.6	2033.5764	-165.4±2.4	2132.7212	-18.7±3.0
1979.7664	-62.8±2.9	2036.7463	-115.0±2.7	2033.7145	-76.7±3.1	2133.4828	-52.6±3.1
1979.7708	-64.6±2.8	2037.7194	-62.7±1.8	2033.7180	-71.9±3.2	2133.4933	-56.8±3.2
1979.7743	-59.9±2.9	2037.7264	-57.9±1.8	2033.7215	-73.6±3.1	2133.5459	-42.0±2.6
1982.7785	-13.9±3.4	2037.7341	-50.8±1.7	2033.7438	-54.3±5.5	2133.5565	-44.4±2.6
1982.7820	-9.0±3.7	2037.7388	-53.5±3.6	2033.7473	-39.3±6.1	2133.6730	-50.5±2.2
2032.5857	85.9±2.3	2128.4616	12.4±3.1	2034.6777	-107.5±1.9	2133.6835	-52.0±2.2
2033.5114	-35.4±3.4	2128.4652	8.5±3.0	2034.6829	-119.7±3.3	2182.6964	-18.9±1.9
2033.5149	-35.6±3.9	2129.3915	-35.4±6.3	2128.4364	-31.7±4.8	2182.7070	-17.7±1.8
2033.5193	-38.7±3.7	2129.3951	-39.4±3.5	2128.4400	-37.7±4.9	2183.7615	-45.2±2.3
2129.3764	42.3±6.5	2183.3209	-59.3±2.8	PG1743+477		2183.7686	-41.7±4.6
2129.3800	7.6±10.5	2183.3245	-60.0±2.6	1653.7123	38.9±2.2	2184.6462	4.9±2.1
PG1619+522		PG1716+426		1653.7220	28.9±2.3	2184.6567	7.3±3.2
1646.7032	-69.3±3.7	1646.7552	-53.1±2.4	1655.6932	39.8±1.9	2187.7147	-28.1±2.2
1646.7081	-76.0±3.6	1651.5972	59.6±2.5	1655.7029	45.9±1.9	2187.7253	-21.7±2.2
1651.5444	-67.1±3.5	1651.6078	49.2±2.6	1656.7376	45.7±2.2	KPD1946+4340	
1651.5518	-68.1±3.7	1657.7333	-73.2±2.1	1656.7474	50.1±2.3	2130.4461	104.4±2.8
1653.6887	-35.0±4.3	1657.7481	-71.3±2.1	1946.7770	-183.7±2.7	2130.4601	130.0±2.9
1653.6937	-40.4±4.2	1946.7530	31.9±3.1	1946.7880	-183.7±2.6	2131.4134	-13.6±3.0
1946.7090	-33.4±3.3	1946.7640	30.8±3.5	2032.6488	39.6±1.4	2131.4274	-46.2±2.8
1946.7164	-29.2±3.2	1977.7568	-59.3±2.1	2032.6645	32.0±2.0	2131.4652	-119.9±4.5
1977.7384	-20.9±2.2	1979.7514	-12.3±2.2	2033.4885	-100.8±3.0	2131.4723	-137.1±4.5
1979.7005	-16.5±2.5	2032.6807	-71.9±2.1	2033.4989	-88.3±2.7	2131.4794	-147.2±4.5
2033.5868	-89.0±2.3	2033.5284	67.1±2.3	2035.6308	17.4±2.1	2131.4865	-158.8±4.4
2033.7010	-90.6±2.5	2184.3237	24.0±4.3	2035.6412	28.9±2.0	2131.5994	-44.7±4.8
2034.6621	-75.5±1.9	2184.3273	31.9±4.3	2035.6894	53.9±1.6	2131.6065	-28.6±4.8
2035.5945	-65.9±1.9			2035.6998	59.1±1.7	2184.4898	-43.5±3.4
				2188.3633	27.4±2.8	2184.4969	-24.8±3.5
				2188.3669	30.5±2.8	2187.5088	49.8±3.7
						2187.5159	26.5±3.7

with $w_i = 1/\sigma_i^2$, where σ_i is the uncertainty on the i -th point and $c_i = \cos(2\pi ft_i)$, $s_i = \sin(2\pi ft_i)$ where t_i is the time of the i -th point; V_i is the measured radial velocity for the i -th point. The term inside the brackets of the exponential is equal to the difference in χ^2 between adopting a constant velocity model versus a model of a constant plus a sinusoid, $\chi_c^2 - \chi_s^2$. That is, it is a measure of the gain one makes by adding a sinusoid to a constant model. Since the constant model χ_c^2 is independent of frequency, this is

the justification for our statement in the main text that the probability of a certain period is dominated by the term $\exp -\chi^2/2$.

Already some assumptions have gone into this result which is the end product of integrating over the systemic velocity and the sine and cosine amplitudes for a given frequency. In particular we took the prior probabilities over these parameters to be uniform in a box extending from $-R_\gamma$ to $+R_\gamma$ in systemic velocity, and $-R_K$ to $+R_K$ in each of

the semi-amplitudes (a factor 4 has entered into Eq. A1 compared to the original version from Marsh, Dhillon & Duck (1995) to account for a factor 2 change in our definition of these ranges). We continue to adopt this prior, largely because it then leads to a tractable integral, but also because it is hard to justify any particular choice of prior, and so one might as well adopt the simplest (although see below for more on this).

Eq. A1 is correct, given our assumptions, as long as the volume of integration wholly encloses the integrand in the systemic velocity/semi-amplitude space. The integrand is a 3D Gaussian centred upon the best-fit values. For good enough data, this will occupy a small region, comparable in dimension to the uncertainties quoted on these parameters. At least this is the case for the best-fit frequency, but it is less clear that it will always be the case. To account for the case where a significant fraction of the integrand lies outside the integration region, we wrote a program that calculated the value of Eq. A1 and, in addition, a correction to it from a Monte Carlo integration. Essentially this computes the fraction of the integrand lying outside the volume of integration. A detail was that we changed the volume of integration to a cylinder with axis along the systemic velocity axis and radius R_K , which gives a uniform prior in orbital phase as one expects. The Monte Carlo work was carried out by computing the eigenvalues and eigenvectors of the matrix \mathbf{A} and then generating points scattered around the maximum using Gaussian random number generators to define the multiple of each eigenvector to use. The correction factor was then the ratio of the number of points that fell within the volume of integration to the total number of points generated. In practice our data was good enough that none of this made much difference to the results.

We adopted a value of $R_\gamma = 500 \text{ km s}^{-1}$ and set R_K by taking the maximum companion mass to be $1.5 M_\odot$. There is certainly a case for having a prior in the systemic velocity that falls off more gradually from a peak close to zero. A Gaussian for example could still be accommodated analytically by a small modification of the matrix \mathbf{A} , however we feel that the greater ease of understanding of a uniform prior is an advantage that should not be wasted. What this means in practice is that we will over- or under-estimate the probabilities listed in Table 3 according to whether the best-fit systemic velocity is far from or close to zero velocity. This is a quantitative manifestation of the lack of confidence one would have in an orbit with a systemic velocity of, say, 2000 km s^{-1} compared to a more moderate one. Similar remarks apply to the prior for K . The uncertainty over the priors is why the final probabilities are themselves subject to uncertainty.

The final step was to integrate the probability as a function of frequency over ranges of frequency. The only technical difficulty here is that the integrand over frequency is extremely peaky with large ranges of very low probability pierced by narrow spikes of high probability. There is little one can do about this apart from computing the integrand over a very finely spaced series of frequencies. We applied straightforward trapezoidal integration, halving the spacing of the frequency grid until the integral converged. Typically this required of the order of one million points, but did not take overly long on any one object. The same points about the systemic velocity and semi-amplitude priors applies to

the prior over frequency. We took a prior uniform in frequency, but this has no particular justification. The final probability is uncertain to the extent that this prior deviates from reality. A factor of 10 would not especially surprise us here.